Research Article

Seasonality of C$_4$ plant growth and carbonate precipitation in the Chinese Loess Plateau may cause positive carbon isotope anomalies in pedogenic carbonates

Yang Fu[1,2] 🔴, Zhengtang Guo[1,2,3] and Guoan Wang[4]

[1]Key Laboratory of Cenozoic Geology and Environment, Institute of Geology and Geophysics, Chinese Academy of Sciences, Beijing 100029, China; [2]University of Chinese Academy of Sciences, Beijing 100049, China; [3]CAS Center for Excellence in Life and Paleoenvironment, Beijing 100044, China and [4]Beijing Key Laboratory of Farmland Soil Pollution Prevention-control and Remediation, College of Resources and Environmental Sciences, China Agricultural University, Beijing 100193, China

Abstract

Carbon isotope analysis of pedogenic carbonate ($\delta^{13}C_{Carb}$) and soil organic matter ($\delta^{13}C_{TOC}$) is widely applied in reconstructions of terrestrial paleovegetation. The $\delta^{13}C$ of different archives is considered well matched and equally reflects the proportion of C$_3$/C$_4$ plant biomass covering the soil profile. However, modern soil and paleosol sequences provide substantial evidence that $\delta^{13}C_{Carb}$ and $\delta^{13}C_{TOC}$ do not always match, raising doubts about the accuracy of quantitative C$_4$ plant reconstructions. Here we report paired $\delta^{13}C$ records of pedogenic carbonates and organic matter occluded within carbonate nodules from the Shaozhai section in the central Chinese Loess Plateau (CLP). The $\delta^{13}C_{Carb}$ record exhibits a positive anomaly and exceeds the theoretical fractionation range with the coexisting $\delta^{13}C_{TOC}$ record during the expansion of C$_4$ plants. The possibility of contamination by detrital carbonates and atmospheric CO$_2$ affecting $\delta^{13}C_{Carb}$ was ruled out based on the morphological features, mineral fractions, and geochemical composition of carbonate nodules. Our study suggests that the enhanced respiration of C$_4$ plants during pedogenic carbonate precipitation may have caused positive shifts in $\delta^{13}C_{Carb}$ records, supporting the hypothesis that the discrepancy in carbon sources explains the $\delta^{13}C_{Carb}$ positive anomaly. Thus, the $\delta^{13}C_{Carb}$ could reflect the maximum relative abundance of C$_4$ plants during their metabolic peaks.

Keywords: Carbon isotope, Pedogenic carbonate, Soil organic matter, the Chinese Loess Plateau, Seasonality, C$_4$ plants

(Received 3 March 2023; accepted 30 October 2023)

INTRODUCTION

The majority of terrestrial vascular plants can be categorized as C$_3$ or C$_4$ plants according to their photosynthetic pathways (Hatch and Slack, 1970), with the former being the most common and ancestral type of photosynthesis (Maeda and Fernie, 2021). Atmospheric CO$_2$ diffuses into the mesophyll cells of C$_3$ plants in response to concentration gradients and directly occupies carbon fixation sites within the cells (Hatch and Slack, 1970). This process is susceptible to photorespiration and leads to the consumption of photosynthate, which is enhanced by increasing temperature and light intensity (Sage et al., 2012). In contrast, the C$_4$ photosynthetic pathway begins with the temporary fixation of intracellular CO$_2$ into a four-carbon intermediate compound. These intermediate compounds are gathered and pumped into bundle sheath cells, releasing CO$_2$ in high concentrations at carbon fixation sites (Hatch and Slack, 1970; Ehleringer and Monson, 1993). By spatially separating the carbon fixation and the Calvin cycle, C$_4$ plants suppress photorespiration and increase the efficiency of photosynthesis (Sage et al., 2012). Therefore, C$_4$

plants have a unique ecological significance due to carbon assimilation advantages under high temperature and light-intensity conditions (Pearcy and Ehleringer, 1984). The origins and expansion of C$_4$ plants reflect combinations of significant environmental and climatic events (Ehleringer et al., 1991; Edwards et al., 2010). Distinct carbon isotope discrimination mechanisms across photosynthetic pathways result in significant $\delta^{13}C$ disparity between C$_3$ and C$_4$ plants (O'Leary, 1981; Farquhar et al., 1982, 1989). The $\delta^{13}C$ of soil organic matter and pedogenic carbonate are thus powerful proxies in documenting the variation of C$_3$/C$_4$ plants and have been widely used in paleovegetation reconstruction (Cerling et al., 1997; An et al., 2005; Edwards et al., 2010; Sun et al., 2012; Carrapa et al., 2019).

Pedogenic carbonates and soil organic matter are the most common archives in terrestrial sediments, inheriting the $\delta^{13}C$ signal of in situ vegetation (Cerling, 1984). The $\delta^{13}C$ of pedogenic carbonates ($\delta^{13}C_{Carb}$) should match the $\delta^{13}C$ of coexisting organic matter ($\delta^{13}C_{TOC}$), which has been well constrained by the theoretical model of Cerling (1984) and its subsequent modifications (Davidson, 1995; Quade et al., 2007). Pedogenic carbonates are generally formed by the dissolution and re-precipitation of primary carbonates by soil water and soil-respired CO$_2$. Thus, the carbon isotope difference ($\Delta^{13}C$) between soil organic matter and pedogenic carbonates mainly comes from isotopic fractionation during two processes: (1) the diffusion of soil-respired

CO_2 within soil pores, producing a positive fractionation of 4.2–4.4‰ (Cerling, 1984; Davidson, 1995); and (2) the precipitation of carbonates from the soil solution, accompanied by isotopic exchanges between the carbonate phase and dissolved CO_2 (Cerling, 1984; Cerling and Quade, 1993). At the isotopic equilibrium state, carbonates are enriched in ^{13}C relative to soil CO_2 by 9–12‰ within a temperature range of 0–25°C (Romanek et al., 1992). The total isotopic difference between pedogenic carbonates and soil-respired CO_2 is expected to fall within a range of approximately 14–17‰ (Cerling and Quade, 1993; Quade et al., 2007; Zamanian et al., 2016). Surveys of modern soils have also confirmed this prediction, with $\delta^{13}C_{Carb}$ values generally being 14–17‰ more positive than those of coexisting $\delta^{13}C_{TOC}$ (Cerling and Quade, 1993; Amundson et al., 1998). Hence, the $\delta^{13}C$ offset ($\Delta^{13}C$) of 14–17‰ is frequently applied in assessing the reliability of paired $\delta^{13}C$ records in paleosol sequences (Cerling et al., 1989; Cerling and Quade, 1993; Sheldon and Tabor, 2009). However, a growing body of research has observed $\Delta^{13}C$ exceeding this theoretical range (Rao et al., 2006; Sanyal et al., 2010; Agrawal et al., 2012; Vögeli et al., 2017; Ghosh et al., 2018), leading to uncertainty in comparing quantitative reconstructions of C_4 vegetation between different archives.

Previous studies have mainly attributed the positive $\Delta^{13}C$ anomaly to the contamination of pedogenic carbonates by external carbon sources, such as the mixing of detrital carbonates from dust sources or the infiltration of atmospheric CO_2 into the soil profile (Cerling, 1984; Rao et al., 2006; Sun et al., 2012; Da et al., 2020). However, this hypothesis cannot explain some observations in monsoon regions. In these cases, carbonates have a pedogenic origin, and the $\delta^{13}C_{TOC}$ value indicates a mixed C_3/C_4 vegetation (Wang and Follmer, 1998; Sinha et al., 2006; Sanyal et al., 2010; Agrawal et al., 2012; Shu et al., 2021). The accumulation of soil organic matter continues with vegetation growth, and $\delta^{13}C_{TOC}$ represents the long-term average isotopic composition of the total plant biomass (Rao et al., 2017). While the precipitation of pedogenic carbonates in monsoon regions is generally concentrated in warm seasons, $\delta^{13}C_{Carb}$ inherits the $\delta^{13}C$ of soil-respired CO_2 during the same period (Peters et al., 2013; Kelson et al., 2020). In a mixed C_3/C_4 ecosystem, C_4 plants with improved photosynthetic efficiency under high temperatures make an enhanced contribution to rhizosphere respiration and cause ^{13}C enrichment in respired CO_2 (Breecker et al., 2009; Shimoda et al., 2009; Huth et al., 2019). Consequently, the soil-respired CO_2 during the pedogenic carbonate formation is biased toward respiration contributed by C_4 plants, resulting in the C_4 plant signal being overrepresented in the $\delta^{13}C_{Carb}$ record. This hypothesis requires further testing, because existing studies mainly focus on the theoretical calculation of fractionation processes and the cross-comparison of $\delta^{13}C$ records in modern soil (Monger et al., 2009; Montañez, 2013; Fischer-Femal and Bowen, 2021; Sarangi et al., 2021), with few considering paleosol sequences over long timescales.

In this study, we analyzed $\delta^{13}C_{Carb}$ and coexisting $\delta^{13}C_{TOC}$ records of the Shaozhai section in the central Chinese Loess Plateau (CLP) since the Pliocene. We made efforts to exclude the contribution of external carbon sources to carbonates by utilizing a range of morphological, mineralogical, and geochemical evidence. We also analyzed the isotopic composition of pedogenic carbonates to evaluate any seasonal bias in carbonate formation. Our aim was to test the hypothesis that variations in carbon sources are responsible for the positive $\Delta^{13}C$ anomaly and to investigate the mechanism underlying this phenomenon. This

study offers novel insights into comprehending the environmental implications of $\delta^{13}C$ records associated with depositional biases and contributes to accurately utilizing the $\delta^{13}C$ proxy in paleovegetation reconstruction.

MATERIALS AND METHODS

### Study area and sampling

The modern CLP is dominated by mixed grassland ecosystems comprising C_3 plants and C_4 plants (Wang and Ma, 2016). Most C_4 plants are warm-climate grasses belonging to the Poaceae, such as *Bothriochloa ischaemum* and *Setaria viridis*, followed by species from the Chenopodiaceae, such as *Salsola collina* (Wang et al., 2008). On the other hand, C_3 plants in this region include herbaceous plants, shrubs, and woody plants, among which herbaceous species from the Poaceae and Compositae have the widest distribution (Jiang and Ding, 2005; Liu et al., 2005). The abundance of C_3 shrubs gradually increases with aridity, and they prevail in the northwest of the CLP. Woody species of *Pinus* and *Ulmus* can be found in the southeastern region and deep gullies or low river terraces (Jiang et al., 2013). The relative abundance of C_4 plants in the modern CLP region increases from around 10% in the northwest to more than 60% in the southeast, as revealed by field investigations (An et al., 2005; Rao et al., 2017). This pattern corresponds with the increasing trend of modern annual temperature and precipitation from northwest to southeast.

The Shaozhai section (34°59.68′N, 107°48.61′E) is located in the Gansu Province of China, which lies in the central CLP and has a typical monsoon climate (Fig. 1). The climate of this region is characterized by warm, humid summers and cold, dry winters. July is the hottest month, and December is the coldest. During 1981–2010, the average summertime (June–August) temperature was 22.7°C, and the average wintertime (December–February) temperature was −0.7°C. The average annual temperature and precipitation were 10.4°C and 694 mm, respectively, with approximately 55% of the total annual precipitation occurring in summer (http://data.cma.cn).

The Shaozhai section comprises a continuous aeolian deposit of 225 m from the base to the top, covering the middle Pliocene to the Quaternary (Cheng et al., 2014; Lv et al., 2022). The Pliocene red clay is generally marked by stronger reddening, finer grain size, and lower porosity than the overlying Quaternary sequence, which exhibits a noticeable color difference between reddish paleosol layers and yellowish loess layers (Lv et al., 2022). However, loess and paleosol layers in the Pliocene red clay exhibit only a slight color difference, with paleosol being mainly reddish-brown or dark brownish and loess layers being yellowish-brown or brownish (Cheng et al., 2014). The Pliocene red clay formation typically has a diffuse boundary between loess–paleosol layers, unlike the distinct boundary observed in the Quaternary consequences. These features indicate that the red clay formation has experienced stronger pedogenesis under a warm and stable climate, making weathered loess layers difficult to distinguish from soil units. Therefore, the red clay formation is divided into extremely thick soil units containing multiple soil B and carbonate nodule horizons (Supplementary Fig. 1).

Carbonate nodules in the upper part of the Quaternary sequence are generally embedded at the bottom of the paleosol layer or the top of the underlying loess layer. They have regular ellipsoidal or irregular tubular shapes with diameters ranging
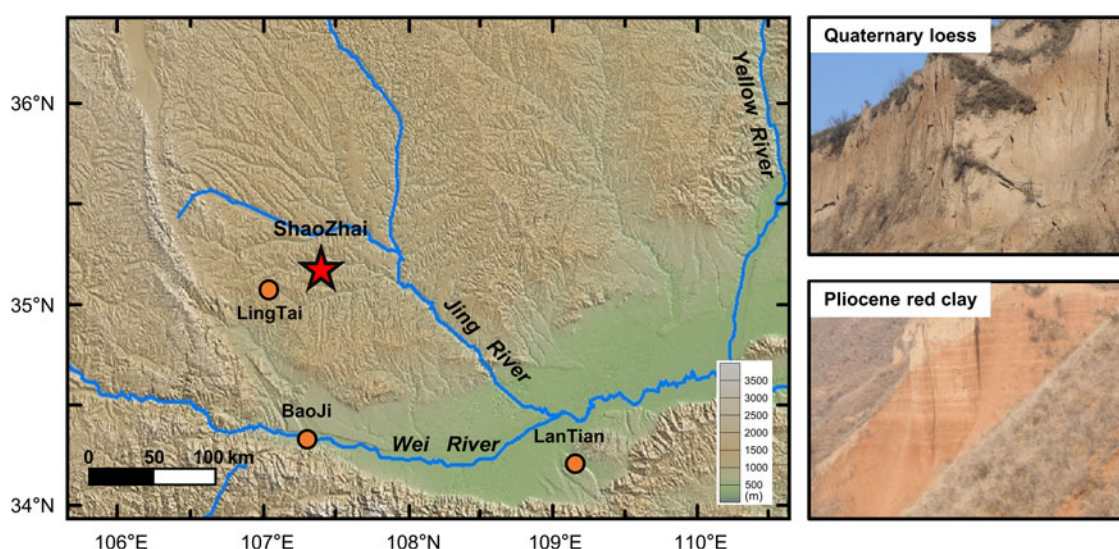
Figure 1. Geographic map of the sections discussed in this study (left) and photographs of the Shaozhai section (right). The red star shows the location of Shaozhai section, and the orange circles indicate the other sections in the Chinese Loess Plateau with comparable published isotope records (An et al., 2005; Da et al., 2015). Photographs of the Shaozhai section depict the interbedded loess–paleosol sequence in the upper part and the relatively uniform red clay formation in the lower part.

from 5 to 10 cm. Cracks and Fe-Mn films are observable within the nodules. The surfaces of some nodules are slightly porous and relatively light in color, while the inner parts are dense, hard, and dark in color. Nodules in the lower part of the Quaternary sequence have a slightly increased diameter, and their morphology is closer to a homogeneous massive structure. Carbonate nodules in the red clay formation are often scattered irregularly in the soil matrix or aggregated in a horizon at the top of weakly developed soil layers. They have uneven surfaces and diameters of 2–5 cm. Some nodules are composed of relatively pure micritic carbonate crystals, resulting in a white color (Supplementary Fig. 1).

To prevent potential contamination of the regolith, trenches (0.5–1 m deep) were dug into the section outcrop to expose fresh aeolian deposits. We applied different sampling strategies for collecting bulk samples and pedogenic carbonate samples. The soil matrix within each soil unit was selected for bulk samples to ensure representativeness and avoid interference from large nodules. Bulk samples were collected at intervals of 10 cm for magnetic susceptibility testing to complete stratigraphic correlation and establish the age model of this profile. When collecting pedogenic carbonate samples, we strove to cover each soil unit and choose ellipsoidal nodules with a complete shape, hard texture, and 2–7 cm diameter. We collected 137 pedogenic carbonate samples to analyze stable isotopes and carbonate mineralogical and elemental composition.

Magnetic susceptibility analysis and chronological framework

Bulk samples were dried and weighed into 10.0 g subsamples for low-frequency magnetic susceptibility testing using a Bartington MS2 magnetic susceptibility meter (Bartington Instruments, Oxfordshire, UK) at a frequency of 0.47 kHz. Each sample was independently measured three times, and a total of 2257 samples were tested. The magnetic susceptibility analyses were conducted at the Laboratory of Soil Structure and Mineralogy, Institute of Geology and Geophysics, Chinese Academy of Sciences.

A previous study of magnetostratigraphy has been carried out in this section, and the pedostratigraphic division of our sampling sequence is consistent with the published results (Qi et al., 2021). Therefore, the age control points were obtained by comparison of magnetic susceptibility records, and the continuous age–depth model was derived by the interpolation method of Kukla et al. (1988). Our section spanned the interval from 0.1 to 4.5 Ma. The detailed comparison of magnetic susceptibility records is presented in Supplementary Figure 2.

Analyses of carbonate mineral and elemental composition

We randomly selected 16 carbonate nodules to analyze the carbonate mineral and elemental composition. These nodules were washed and dried, then mechanically crushed. The core fragments were ground in an agate mortar until the particle diameter was less than 45 μm. X-ray diffraction (XRD) analyses for mineral composition of powdered samples were conducted with a PANalytical diffractometer (Malvern Panalytical B.V., Almelo, Netherlands) with Ni-filtered Cu-Kα radiation (40 kV, 40 mA). For elemental analysis, an appropriate amount of powder was placed in a plastic centrifuge tube with 0.2 mol/L acetic acid overnight to dissolve the carbonate fraction. The Mn, Mg, and Ca in the dissolved product were measured by inductively coupled plasma mass spectrometry (PerkinElmer, Waltham, MA, USA) to obtain the elemental concentration. Analytical precision is less than 4% for Mn/Ca and Mg/Ca ratios. The XRD and elemental composition analyses were conducted at the Laboratory of Soil Structure and Mineralogy, Institute of Geology and Geophysics, Chinese Academy of Sciences.

Stable isotope analysis

A total of 137 pedogenic carbonate samples were washed repeatedly with pure water and scrubbed to remove soil attached to their surfaces. To avoid potential heterogeneity in micro-sampling, the nodule was cut, and the core part was broken into pieces, from

which about 5 g of subsamples were ground to below 200 mesh and thoroughly mixed before further analysis. Samples were divided into two groups, one of which was used for the measurement of the carbon and oxygen isotope ratio ($\delta^{13}C_{Carb}$ and $\delta^{18}O_{Carb}$) by a Thermo-Finnigan MAT-253 isotope ratio mass spectrometer (Thermo Scientific, Waltham, MA, USA) coupled with the Gasbench carbonate device (Thermo Scientific) reacted at 75°C with the oversaturated H_3PO_4. Following the conventional stable isotope analysis protocol (Thomas, 1991), we performed one test on most samples and incorporated repeated tests on duplicate samples and different internal standards. Results are reported in per mil (‰) notation relative to the Vienna Pee Dee Belemnite (VPDB). Every eighth sample was treated as a replicate, and two laboratory internal standards with known isotopic values (GBW04416, $\delta^{13}C_{VPDB} = +1.61‰$, $\delta^{18}O_{VPDB} = -11.59‰$; GBW04417, $\delta^{13}C_{VPDB} = -6.06‰$, $\delta^{18}O_{VPDB} = -24.12‰$) were added for repeated testing. The standard deviation was thus obtained for the whole data set, and it was better than 0.15‰ for the $\delta^{13}C_{Carb}$ measurements and better than 0.20‰ for the $\delta^{18}O_{Carb}$ measurements.

The other group of samples was put into a centrifuge tube and reacted with 6 N HCl for 48 h to remove carbonates. Then, deionized water was added to rinse samples until neutral and freeze-dried. The residue of each sample was wrapped in a tin cup, and the carbon isot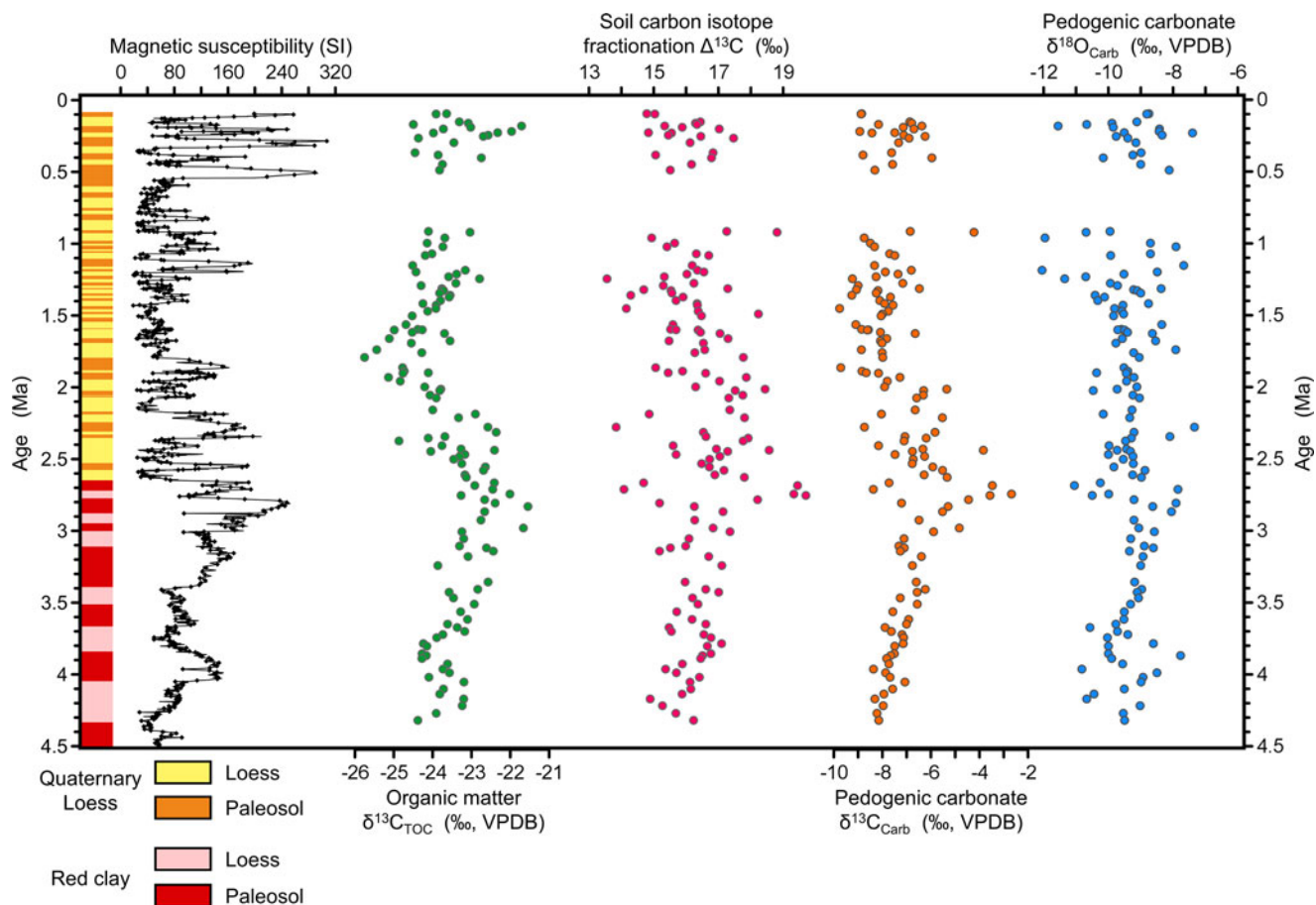ope ratio of organic matter occluded within the carbonate nodule ($\delta^{13}C_{TOC}$) was determined by a MAT-253 isotope ratio mass spectrometer (Thermo Scientific) coupled with a FLASH EA1112 elemental analyzer (Thermo Scientific). We followed the same procedure used in the carbonate isotope analysis, and two laboratory internal standards (GBW04407, $\delta^{13}C_{VPDB} = -22.43‰$; urea, $\delta^{13}C_{VPDB} = -49.1‰$) were used to calibrate carbon isotope results. The standard deviation for measurements of $\delta^{13}C_{TOC}$ was better than 0.2‰ for the whole data set.

Given that the carbon isotopic composition of atmospheric CO_2 ($\delta^{13}C_{atm}$) has varied from the Pliocene to the present day, all raw carbon isotope ratios were corrected for secular changes in $\delta^{13}C_{atm}$ (Tipple et al., 2010; Schmitt et al., 2012). We used the mid-Holocene $\delta^{13}C_{atm}$ of $-6.3‰$ as the basis for this correction.

The stable isotope analyses were conducted at the Laboratory for Stable Isotope Geochemistry, Institute of Geology and Geophysics, Chinese Academy of Sciences.

RESULTS

The magnetic susceptibility result of the Shaozhai section is shown in Figure 2 and Supplementary Table 1. The loess layers have low magnetic susceptibility values and have undergone

Figure 2. Magnetic susceptibility and carbon and oxygen isotope composition of pedogenic carbonates ($\delta^{13}C_{Carb}$ and $\delta^{18}O_{Carb}$), carbon isotope composition of organic matter occluded within carbonate nodules ($\delta^{13}C_{TOC}$), and carbon isotope offset between $\delta^{13}C_{Carb}$ and $\delta^{13}C_{TOC}$ ($\Delta^{13}C$) of the Shaozhai section. Yellow and orange areas in the lithologic column represent the Quaternary loess and paleosol layers, while pink and red areas represent loess–paleosol units of the red clay formation. VPDB, Vienna Pee Dee Belemnite.

weak pedogenesis, whereas paleosol layers have high values due to the pedogenic formation of magnetic minerals.

The $\delta^{13}C_{Carb}$ varied from $-2.6‰$ to $-9.9‰$, with a mean value of $-7.4‰$; the $\delta^{18}O_{Carb}$ varied from $-7.3‰$ to $-12.0‰$, with a mean value of $-9.4‰$; the $\delta^{13}C_{TOC}$ ranged from $-20.4‰$ to $-26.2‰$, with a mean value of $-23.6‰$ (Fig. 2, Supplementary Table 2). The long-term trend of $\delta^{13}C_{TOC}$ is consistent with that of $\delta^{13}C_{Carb}$. Both of them reached the highest values in the entire sequence during 3–2.5 Ma, which coincides with the widespread expansion of C_4 plants in the CLP during the late Pliocene (Ding and Yang, 2000; An et al., 2005; Suarez et al., 2011; Sun et al., 2012; Zhou et al., 2014). However, during this period (3–2.5 Ma), the increase in $\delta^{13}C_{Carb}$ values (approximately 4‰) was greater than that of the less-variable $\delta^{13}C_{TOC}$ (approximately 2‰), causing the isotopic offset between $\delta^{13}C_{Carb}$ and $\delta^{13}C_{TOC}$ ($\Delta^{13}C$) to exceed the theoretical range of 14–17‰ (Fig. 2).

The XRD results of nodule samples showed that carbonate fractions in nodules comprise mainly pure calcite minerals (Fig. 3); their Mg/Ca ratios ranged from 9.23 to 26.52 mol/mol, and Mn/Ca ratios ranged from 0.10 to 0.63 mmol/mL (Supplementary Table 3).

DISCUSSION

Interpretation of the $\delta^{13}C_{Carb}$ record

The source and origin of carbonates in aeolian deposits are usually complex, and only the pedogenic carbonate that forms via recrystallization during pedogenesis can faithfully reflect the local vegetation conditions. Abiotic factors, such as the mixing of detrital carbonate from dust sources and the infiltration of atmospheric CO_2 into the soil profile, could also drive increases in $\delta^{13}C_{Carb}$ and $\Delta^{13}C$ values. Therefore, we examine these two influences separately in the following sections.

Influence of detrital carbonates

The coexistence of detrital and pedogenic carbonate in aeolian sequences is sometimes unavoidable due to dust accumulation and incomplete dissolution of soil parent materials (Rao et al., 2006; Sheng et al., 2008). To avoid the potential contamination of detrital carbonates, we carefully selected carbonate nodules with typical pedofeatures, including distinct ellipsoidal outer boundaries and a firm internal structure similar to the soil matrix (Fig. 3A and B). Such morphological features indicate that the carbonate nodules had a purely secondary origin (Barta, 2011; Zamanian et al., 2016).

Furthermore, striking mineralogical and geochemical differences between detrital and pedogenic carbonates can be used to identify potential contamination. In the study area, detrital carbonates carried by dust are mainly from marine carbonate strata in the arid regions of central Asia (Yang and Ding, 2008; Chen and Li, 2011; Zhang et al., 2022). These carbonates inherit the chemical composition of seawater in geologic history and have experienced long-term burial metamorphism. The detrital carbonate usually includes a large proportion of dolomite minerals, with an elemental composition characterized by high Mg/Ca or Mn/Ca ratios (Li et al., 2013; Li and Li, 2014; Meng et al., 2019). However, our XRD results indicate that the carbonate component of our samples is solely composed of calcite with no presence of dolomite observed (Fig. 3A and B). Because the dolomite dissolves more slowly than calcite during the soil weathering process, the disappearance of dolomite indicates the total dissolution of preexisting detrital carbonates (Tribble et al., 1995; Meng et al., 2015). Furthermore, our carbonate samples have particularly low Mg/Ca and Mn/Ca ratios (Fig. 3C), which are significantly lower than those of bulk carbonates from weakly weathered loess layers across the CLP and potential dust source regions, such as modern desert topsoil. In addition, their Mg/Ca and Mn/Ca ratios fall within the same range as those of other carbonates with unquestionable secondary origins, such as rhizoliths, pseudomycelia, and snail shells (Li et al., 2013).
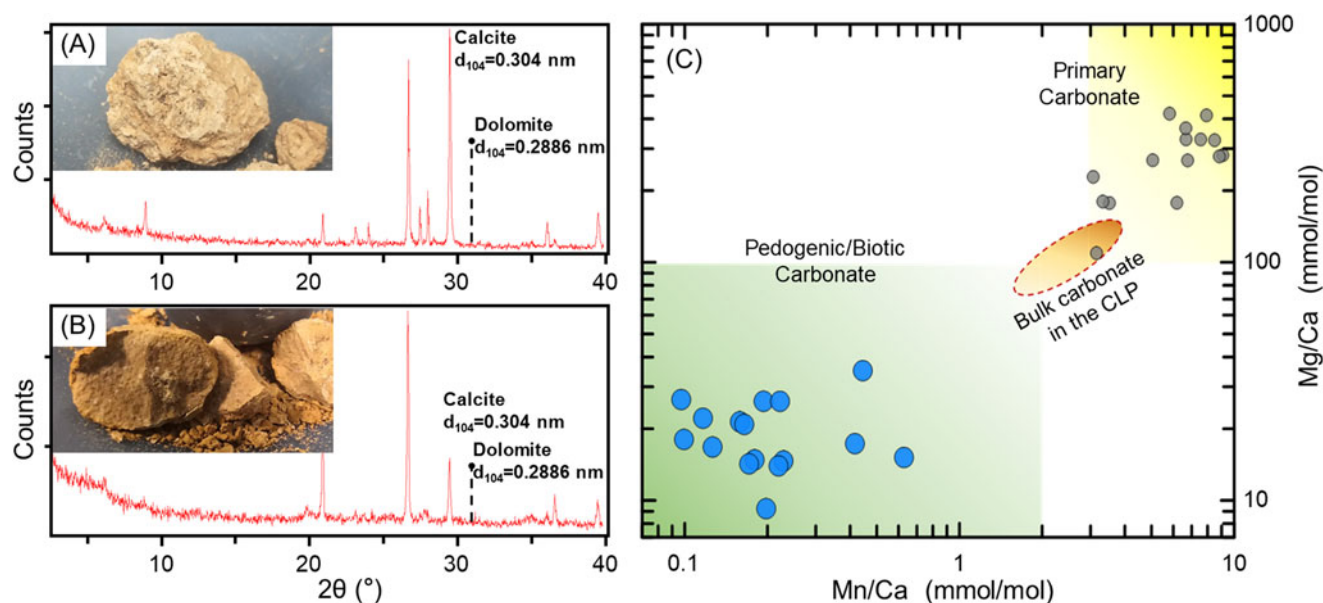
Figure 3. The mineralogical and elemental composition of carbonate nodules from the Shaozhai section. (**A and B**) The X-ray diffractograms of nodule samples and the carbonate mineral were entirely composed of calcites. (**C**) The Mg/Ca and Mn/Ca ratios of our nodule samples (blue circles), bulk carbonates from modern desert topsoils (gray circles and yellow shaded area), L1–S1 layers across the Chinese Loess Plateau (CLP; orange shaded area), the Holocene microcodium and biogenic carbonates (green shaded area). These elemental composition data of different carbonates were obtained from Li et al. (2013) and Li and Li (2014).

The $\delta^{13}C$ and $\delta^{18}O$ of detrital carbonates are close to 0‰ (VPDB), significantly positive compared with those of pedogenic carbonates (Wang et al., 2005; Cao et al., 2008; Sun et al., 2015; Horton et al., 2016). In the CLP region, the $\delta^{13}C$ and $\delta^{18}O$ of pedogenic carbonates are generally below −3‰ (VPDB) and −5‰ (VPDB), respectively (Ding and Yang, 2000; Li et al., 2007; Yang et al., 2012; Luo et al., 2020). The present study observed that all $\delta^{13}C_{Carb}$ and $\delta^{18}O_{Carb}$ of our samples ranged from −2.6‰ to −9.9‰ and from −7.3‰ to −12.0‰, respectively (Fig. 4A and B), differing from the $\delta^{13}C$ and $\delta^{18}O$ values of detrital carbonates.

Furthermore, the incomplete dissolution of detrital carbonates will be most evident in the Quaternary loess layers because of weak pedogenesis and rapid dust accretion (Guo et al., 2004; Sun et al., 2010). Consequently, loess layers will have a higher proportion of detrital carbonates and systematically higher $\delta^{13}C_{Carb}$ and $\delta^{18}O_{Carb}$ values than paleosol layers (Rao et al., 2006; Liu et al., 2011). According to the same principle, the $\delta^{13}C_{Carb}$ and $\delta^{18}O_{Carb}$ values of the Quaternary loess will be higher than those of the Pliocene red clay. However, this study showed that the Quaternary loess has lower $\delta^{13}C_{Carb}$ values and identical $\delta^{18}O_{Carb}$ values compared with the red clay formation. In addition, neither $\delta^{13}C_{Carb}$ nor $\delta^{18}O_{Carb}$ had differences in the range between loess and paleosol (Fig. 4).

Magnetic susceptibility has been suggested as a good indicator of the intensity of pedogenesis in the Quaternary loess–paleosol sequence, and it increases with increasing pedogenesis (Zhou et al., 1990). If detrital carbonates are present in significant amounts, $\delta^{13}C_{Carb}$ or $\delta^{18}O_{Carb}$ values and magnetic susceptibility will exhibit negative correlations, because weak pedogenesis accompanied by higher detrital carbonate contribution leads to an increase in the $\delta^{13}C_{Carb}$ or $\delta^{18}O_{Carb}$ (Rao et al., 2006; Sun et al., 2019). However, our data did not show this negative correlation in the Quaternary loess–paleosol sequence, while positive correlations between $\delta^{18}O_{Carb}$ and magnetic susceptibility were observed (Fig. 4C and D).

An increase in the content of fine-grained ferrimagnetic minerals created by pedogenesis is the primary reason for enhanced magnetic susceptibility in the Pliocene red clay (Hao et al., 2008, 2009). Hence, the higher magnetic susceptibility still indicates relatively stronger pedogenesis (Nie et al., 2007). If detrital carbonates are present in the Pliocene red clay, negative correlations between $\delta^{13}C_{Carb}$ or $\delta^{18}O_{Carb}$ and magnetic susceptibility will also be observed. However, similar to results from the Quaternary loess–paleosol sequence, neither $\delta^{13}C_{Carb}$ nor $\delta^{18}O_{Carb}$ is negatively correlated with magnetic susceptibility, whereas $\delta^{18}O_{Carb}$ is positively correlated with magnetic susceptibility in the Pliocene red clay (Fig. 4A and B).

In summary, mineralogical and geochemical evidence strongly supports the purely pedogenic origin of our carbonate samples and excludes detrital carbonate contamination. Previous studies were conducted on some sections in the central and southern parts of the CLP, which are at the same latitude as the Shaozhai section and far from the northern sandy lands (Yang et al., 2012; Zhang and Liu, 2013). These studies also suggested that the contribution of detrital carbonates is negligible in carbonate nodules, which is consistent with our conclusion.

Influence of atmospheric CO_2

The contribution of ^{13}C-enriched atmospheric CO_2 in the soil atmosphere can be identified by enhanced carbon isotope fractionation between $\delta^{13}C_{Carb}$ and $\delta^{13}C_{TOC}$ (Quade et al., 2007). Modern surveys of pedogenic carbonates and soil organic matter have observed that $\Delta^{13}C$ anomalies occurred at different depths in the soil profile (Retallack, 2009; Montañez, 2013; Myers et al., 2016). The infiltration of atmospheric CO_2 into the soil profile is primarily limited to the surface layer and does not reach soil layers below 50 cm (Cerling, 1984; Quade et al., 2007). Therefore, $\Delta^{13}C$ anomalies in deeper soils are expected to be unrelated to the infiltration of atmospheric CO_2 (Fig. 5). Typical soil
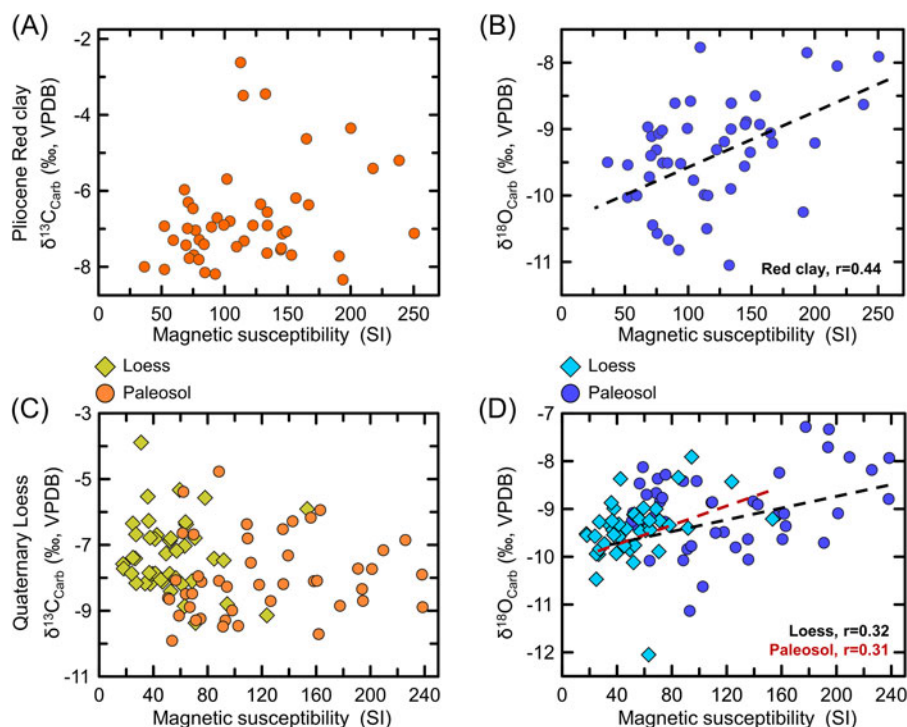
Figure 4. The $\delta^{13}C_{Carb}$, $\delta^{18}O_{Carb}$, and magnetic susceptibility in the Pliocene red clay (**A and B**) and Quaternary loess–paleosol sequence (**C and D**) in the Shaozhai section. VPDB, Vienna Pee Dee Belemnite.
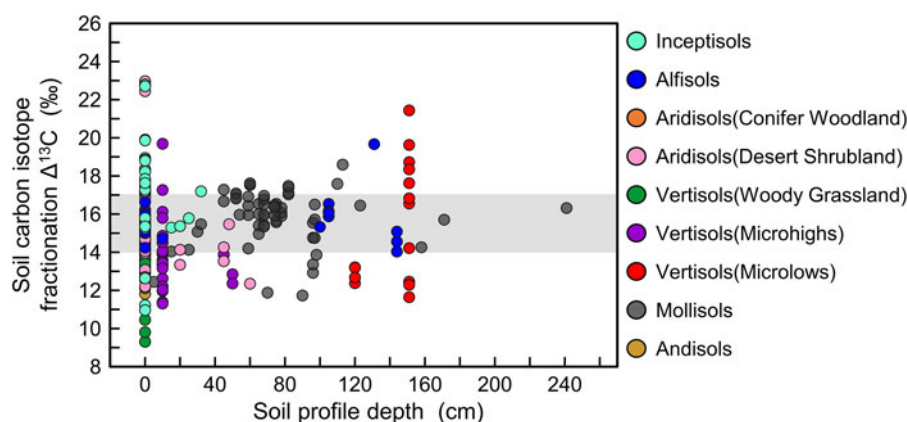
Figure 5. Carbon isotope fractionation with depth in different types of modern soil profiles. The gray shaded area indicates the theoretical range (14–17‰) of $\Delta^{13}C$. Carbon isotope data were compiled from Retallack (2009), Montañez (2013), and Myers et al. (2016).

types in the modern CLP, such as alfisols, aridisols, and mollisols, generally have a depth to the carbonate nodular horizon (Bk) greater than the reach of atmospheric CO_2 (Feng and Wang, 2005; Yang et al., 2012). Moreover, the depth of pedogenic carbonate accumulation is positively correlated with precipitation in semiarid areas (Retallack, 2005; Zamanian et al., 2016), thus further reducing the potential contribution of atmospheric CO_2.

If atmospheric CO_2 infiltrates the interior of the soil profile, then periods with higher atmospheric CO_2 concentrations should be more prone to such infiltration than periods with lower CO_2 concentrations. However, the highest $\Delta^{13}C$ values in this study did not occur during the Pliocene warm period (~3.3 Ma), which had the highest CO_2 concentrations. On the contrary, they occurred during the late Pliocene to the Early Quaternary period, when atmospheric CO_2 dropped sharply (Fig. 6A). Other studies (Fig. 6) have also found that the highest anomalies did not occur during geologic periods when atmospheric CO_2 concentrations were highest (An et al., 2005; Bereiter et al., 2015; Da et al., 2015; Rae et al., 2021).

In addition, loose and porous soil layers are typically more prone to existing atmospheric CO_2 infiltration than dense soil layers. The Quaternary loess layers have coarser particles and higher porosity than the paleosol layers and Pliocene red clay, making them more vulnerable to atmospheric CO_2 infiltration and more likely to produce pronounced $\Delta^{13}C$ anomalies. However, the typical loess layers such as L1, L2, L9, and L15, with the highest dust accumulation rate, higher soil matrix porosity, and lower vegetation productivity, did not show the expected $\Delta^{13}C$ anomalies (Fig. 6A and C).

If such infiltration did occur, $\delta^{13}C_{Carb}$ and $\delta^{13}C_{TOC}$ would unlikely show a consistent trend or strong correlation, because atmospheric CO_2 has a much more positive $\delta^{13}C$ composition than CO_2 generated by plant and soil respiration (Quade et al., 2007). The contribution of atmospheric CO_2 tends to homogenize $\delta^{13}C_{Carb}$ to a fixed value independent of $\delta^{13}C_{TOC}$. However, this and previous studies have shown a positive correlation between the $\delta^{13}C_{Carb}$ and $\delta^{13}C_{TOC}$ for each section (Fig. 6B, D, and E).

Therefore, the evidence from these four aspects allows us to conclude that $\Delta^{13}C$ anomalies are unrelated to atmospheric CO_2 infiltration.

Seasonality of C₄ plant growth and carbonate precipitation controlled $\delta^{13}C_{Carb}$ anomaly

The low biomass of C₄ plants in the Shaozhai section before 3 Ma is suggested by the $\delta^{13}C_{Carb}$ and $\delta^{13}C_{TOC}$ with average values of

−7.3‰ and −23.5‰, respectively, which are in agreement with published pollen and $\delta^{13}C$ records from the CLP (Ding and Yang, 2000; Jiang et al., 2001; An et al., 2005; Ma et al., 2005; Li et al., 2011; Rao et al., 2012a). During this period, our $\delta^{13}C_{Carb}$ and $\delta^{13}C_{TOC}$ records showed a gradual positive trend with small fluctuations (Fig. 2). They maintained the congruent trend and $\Delta^{13}C$ values within the expected range (14–17‰) in glacial cycles and on longer timescales. This demonstrates the consistency in the composition and variations of C₃/C₄ vegetation between the carbonate precipitation period and soil organic matter accumulation period.

At the Pliocene–Quaternary transition, $\delta^{13}C_{Carb}$ and $\delta^{13}C_{TOC}$ experienced a pronounced positive shift and reached their highest values at approximately 2.8 Ma, with the rise in $\delta^{13}C_{Carb}$ being more abrupt than that of $\delta^{13}C_{TOC}$. Both indicate a considerable expansion of C₄ plants, which is also observed in contemporaneous sections throughout the CLP (Ding and Yang, 2000; Jiang et al., 2001; An et al., 2005; Suarez et al., 2011; Rao et al., 2012a). The magnitude of $\delta^{13}C_{Carb}$ positive shift (ca. 4‰) and peak values (ca. −3‰) at the Shaozhai section are similar to what has been reported in previous studies (Ding and Yang, 2000; An et al., 2001; Jiang et al., 2001; Suarez et al., 2011). However, this study and other $\delta^{13}C_{TOC}$ records exhibit a relatively minor positive excursion of 2.0‰ to 2.5‰ (An et al., 2001; Rao et al., 2012a).

The negative correlation between $\delta^{18}O_{Carb}$ and $\delta^{13}C_{Carb}$ became apparent after 2.8 Ma (Fig. 7B and C). Because the isotopic composition of pedogenic carbonates is inherited from meteoric waters and terrestrial vegetation, the relationship between $\delta^{18}O_{Carb}$ and $\delta^{13}C_{Carb}$ reflects the vegetation response to climate changes (Cerling and Quade, 1993; Yang et al., 2012; Kovda et al., 2014; Bayat et al., 2018). In the modern CLP, the monsoon climate results in a concentration of precipitation during warm seasons. Therefore, the oxygen isotope composition of meteoric waters during warm seasons shows a notable negative shift due to the rainfall effect (Vuille et al., 2005), producing a corresponding negative shift in the $\delta^{18}O_{Carb}$ (Zhang et al., 2018). Although C₄ plants maintain high photosynthetic efficiency under high temperatures and water-stressed conditions (Pearcy and Ehleringer, 1984; Sage et al., 2012), severe droughts in growing seasons are unfavorable for their growth, as indicated by the scarcity of C₄ plants in Mediterranean climates (Rao et al., 2012b). High temperatures and increased precipitation during growing seasons, as a result of the intensification of seasonality, benefit C₄ plants by allowing them to fully utilize their adaptive advantages and causing a positive shift in $\delta^{13}C_{Carb}$. Previous surveys
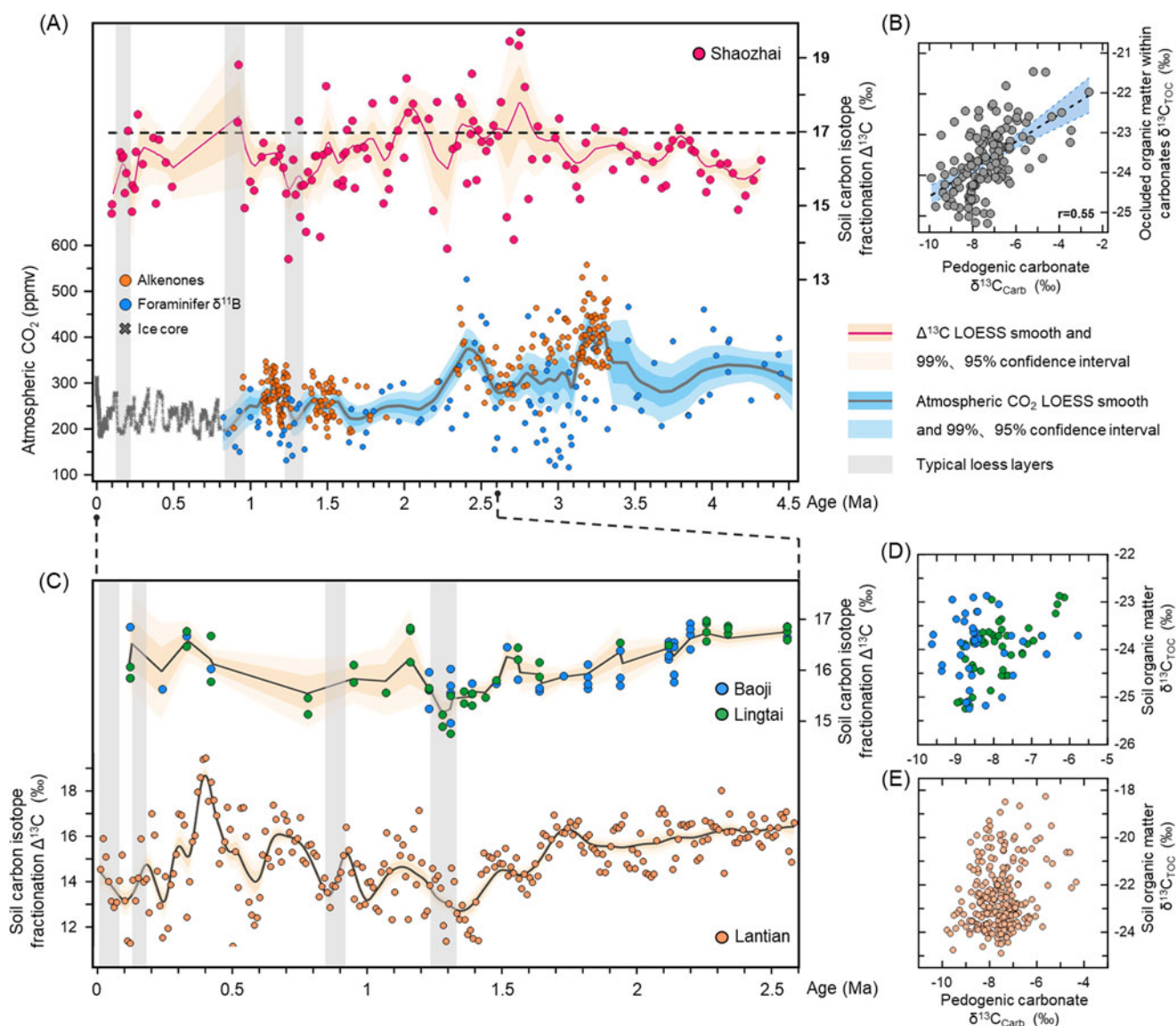
**Figure 6.** Comparison of atmospheric CO_2 concentration and $\delta^{13}C_{Carb}$ and $\delta^{13}C_{TOC}$ records from different sections. (**A**) $\Delta^{13}C$ from the Shaozhai section and the atmospheric CO_2 concentration from the Pliocene; the black dotted line represents the theoretical upper limit of $\Delta^{13}C$ (17‰). (**B**) The $\delta^{13}C_{Carb}$ and $\delta^{13}C_{TOC}$ records of the Shaozhai section. The individual data points with LOESS smoothing in thick solid lines and confidence intervals indicated by shaded areas. The gray shaded bars represent the loess layers L1, L2, L9, and L15. (**C**) $\Delta^{13}C$ from the Baoji, Lingtai, and Lantian sections. (**D and E**) The $\delta^{13}C_{Carb}$ and $\delta^{13}C_{TOC}$ records of each section shown in **C**. Baoji, Lingtai, and Lantian data were collected from An et al. (2005) and Da et al. (2015). The atmospheric CO_2 concentration reconstruction results are compiled from Bereiter et al. (2015) and Rae et al. (2021).

of modern vegetation and the synchronous migration of the C_4 plant distribution boundary and the monsoon rainfall belt have validated this hypothesis (An et al., 2005; Von Fischer et al., 2008; Yang et al., 2015; Munroe et al., 2022). Therefore, pedogenic carbonates generally have a distinct negative correlation between $\delta^{13}C_{Carb}$ and $\delta^{18}O_{Carb}$ in the CLP (Yang et al., 2012). This specific correlation suggests seasonal biases in both the metabolism of C_4 plants and pedogenic carbonate formation, and it precludes the potential contamination of detrital carbonates and atmospheric CO_2.

Simultaneous with the rapid rise in our $\delta^{13}C_{Carb}$ record at 2.8 Ma, the $\Delta^{13}C$ value of the Shaozhai section starts to show abnormally high values exceeding 17‰ because of larger variations in $\delta^{13}C_{Carb}$ compared with $\delta^{13}C_{TOC}$ (Fig. 7C). Given that we have excluded external contamination, soil CO_2 produced by plant root respiration and decomposition of soil organic matter is considered

the primary carbon source that contributes to pedogenic carbonates (Cerling, 1984; Zamanian et al., 2016). Consequently, the increased range of $\delta^{13}C_{Carb}$ variation implies that greater vegetation changes occurred during periods of carbonate precipitation than those of organic matter accumulation. During warm seasons, root respiration dominates the soil CO_2 due to vigorous plant metabolism (Hanson et al., 2000; Bond-Lamberty and Thomson, 2010). The respiration flux contributed by C_3 and C_4 plants at certain times probably does not match their respective proportions in annual plant biomass, because the competitive advantage of C_3 and C_4 plants differs seasonally (Lai et al., 2006; Shimoda et al., 2009). In mixed C_3/C_4 grassland ecosystems, the contribution of C_4 plants to root respiration is greater in warm seasons than in other seasons due to their higher temperature tolerance and water-use efficiency (Pearcy and Ehleringer, 1984). High-resolution field observations have also
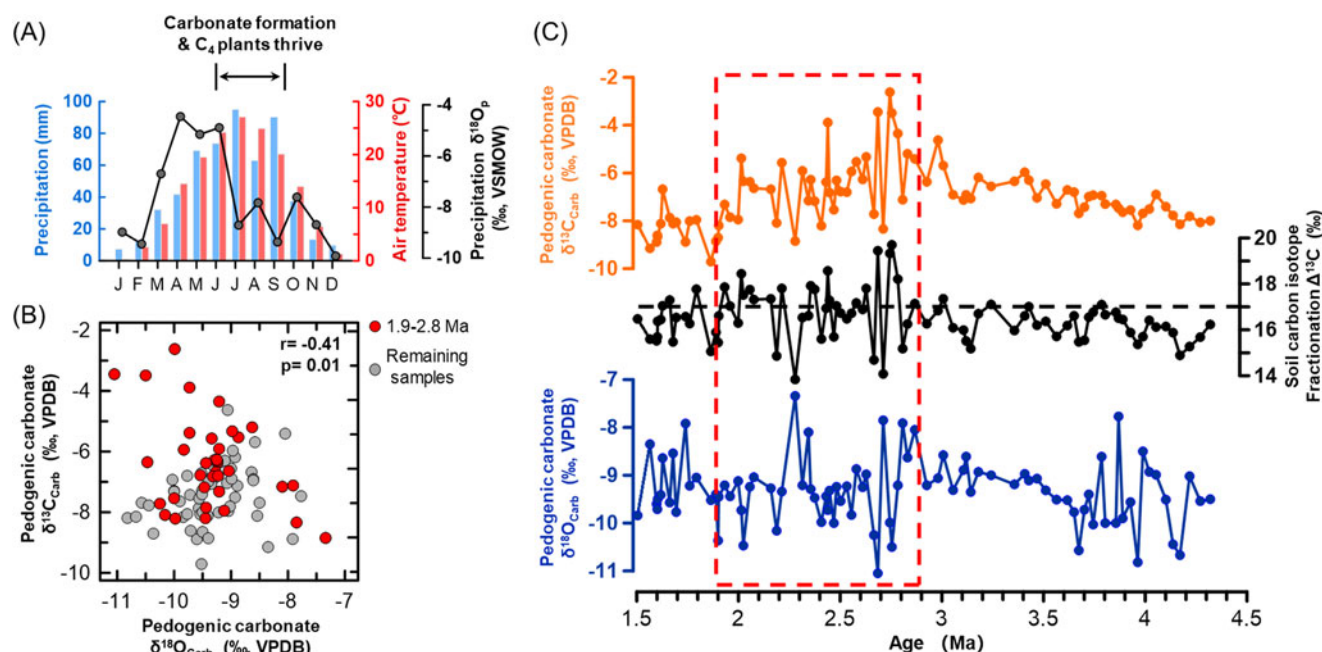
Figure 7. Modern meteorological data in the Chinese Loess Plateau and $\delta^{13}C_{Carb}$, $\delta^{18}O_{Carb}$, and $\Delta^{13}C$ records of the Shaozhai section during the late Pliocene C_4 expansion event. (**A**) The monthly average temperature (red), precipitation (blue), and monthly weighted precipitation $\delta^{18}O_p$ (black) of GNIP site Xi'an (IAEA/WMO, 2006). (**B**) The $\delta^{13}C_{Carb}$–$\delta^{18}O_{Carb}$ correlation of pedogenic carbonates ($P = 0.01$, $r = -0.41$). Red circles indicate samples exhibiting a negative $\delta^{13}C_{Carb}$–$\delta^{18}O_{Carb}$ correlation with high $\Delta^{13}C$ values in the red dashed box of **C**. (**C**) The $\delta^{13}C_{Carb}$, $\delta^{18}O_{Carb}$, and $\Delta^{13}C$ variation of the Shaozhai section; the black dotted line represents the theoretical upper limit of $\Delta^{13}C$ (17‰).

confirmed apparent seasonal cycles in the carbon isotope composition of soil-respired CO_2 (Breecker et al., 2009, 2012; Huth et al., 2019). Therefore, the $\delta^{13}C$ of soil CO_2 in warm seasons overrepresents the abundance of C_4 plants as a result of their increased metabolism, which is documented by pedogenic carbonates. We speculate that this mechanism could explain high $\Delta^{13}C$ values observed in the present study after 2.8 Ma.

From 2.8 to 1.5 Ma, the $\delta^{13}C_{Carb}$ and $\delta^{13}C_{TOC}$ in the Shaozhai section started to decrease and reached a minimum, indicating a decline in C_4 plants. This decline also occurs in the central and western parts of the CLP and is believed to be primarily caused by the long-term cooling trend associated with enhanced Northern Hemisphere glaciation (Ding and Yang, 2000; An et al., 2005; Suarez et al., 2011; Sun et al., 2012). According to surveys of $\delta^{13}C$ end-member values of modern C_3/C_4 plants and correction for secular changes in atmospheric $\delta^{13}C_{CO2}$ (+1.7‰), we select −25‰ and −8‰ as the most conservative thresholds for $\delta^{13}C_{Carb}$ and $\delta^{13}C_{TOC}$ indicating pure C_3 plants (Wang et al., 2008; Tipple et al., 2010; Rao et al., 2017; Jiang et al., 2019), both of which are widely accepted and applied in paleovegetation reconstruction (Cerling et al., 1997; Tipple and Pagani, 2007; Edwards et al., 2010). Therefore, our $\delta^{13}C_{Carb}$ and $\delta^{13}C_{TOC}$ values are close to the C_3 plant end-member from 1.9 to 1.5 Ma, suggesting insufficient evidence to support the presence of C_4 plants. Given the positive $\delta^{13}C$ excursion in our record and the distinct $\delta^{13}C_{Carb}$–$\delta^{18}O_{Carb}$ correlation (Fig. 7), anomalous $\Delta^{13}C$ values from 2.8 to 1.9 Ma can be confidently correlated to the emergence and enhanced metabolism of C_4 plants. Pedogenic carbonates inherit the $\delta^{13}C$ of soil-respired CO_2 with a positive bias during the growing season for C_4 plants, leading to abnormally high $\Delta^{13}C$ values that exceed the theoretical range.

After 1.5 Ma, our $\delta^{13}C_{Carb}$ and $\delta^{13}C_{TOC}$ records maintain a good consistency and experience a rebound with slow positive

shifts continuing into the Late Quaternary. Despite $\delta^{13}C$ records in the Shaozhai section being interrupted due to the complete leaching of carbonate in some well-developed paleosol layers such as S5–S8, they still attain relatively high values after 0.5 Ma. It shows that the abundance of C_4 plants resumed a slow increase with the strengthening of the summer monsoon and finally reached a significant proportion in this region again. Although some high values of $\Delta^{13}C$ are also present during this period (Fig. 6), we have refrained from employing the same mechanism to explain these anomalies out of caution. The credibility of several high $\Delta^{13}C$ values in our record at 900 and 300 ka is somewhat suspect due to the scarcity of data points. In addition, the lack of a $\delta^{18}O_{Carb}$ record hinders further evaluation of the more obvious $\Delta^{13}C$ anomaly in the Lantian section at 400 ka (An et al., 2005). Therefore, we provisionally conclude that those high $\Delta^{13}C$ values cannot robustly suggest the seasonal thriving of C_4 plants, despite our comprehensive examination of all pedogenic carbonate samples and another evident C_4 plant expansion event in the CLP around 0.5 Ma (Sun et al., 2012; Zhang et al., 2013a; Zhou et al., 2014).

CONCLUSION

This study investigated the discrepancy between $\delta^{13}C$ records of pedogenic carbonate and organic matter occluded within carbonate nodules in the loess–paleosol sequence. It shows that a positive anomaly in $\delta^{13}C_{Carb}$ records mainly occurred in the C_3/C_4 mixed ecosystems and coincided with the expansion of C_4 plants. Contamination of pedogenic carbonates by external carbon sources was precluded through morphological, mineralogical, and geochemical evidence. Consequently, we attribute this discrepancy to the fact that $\delta^{13}C_{Carb}$ mainly records summer vegetation composition, while $\delta^{13}C_{TOC}$ reflects year-round vegetation

composition. Our study suggests that the seasonality of C$_4$ plant growth and carbonate precipitation caused positive carbon isotope anomalies in pedogenic carbonates. Therefore, the δ^{13}C$_{Carb}$ could represent the maximum relative abundance of C$_4$ plants that can be achieved during the C$_4$ plant expansion events. The reconstruction based on pedogenic carbonate can be regarded as an upper limit for the relative abundance of C$_4$ plants.

Our results support the idea that the Δ^{13}C has the potential to characterize climate seasonality (Wang et al., 2004; Sinha et al., 2006; Sanyal et al., 2010). However, its application necessitates a thorough evaluation of the following factors. First, the source of carbonates must be carefully examined to ensure their pedogenic origin and to rule out the influence of atmospheric CO$_2$ contamination during carbonate precipitation. Second, although plants of the same photosynthetic type also exhibit δ^{13}C adjustments due to seasonal variations in temperature and precipitation (Stevenson et al., 2005; Breecker et al., 2009), Δ^{13}C is better suited for use in the mixed C$_3$/C$_4$ ecosystem instead of a pure C$_3$ or C$_4$ ecosystem. Third, the period of carbonate precipitation is essential for interpreting the documented vegetation and climate changes. Pedogenic carbonate records the vegetation composition in warm seasons in midlatitude monsoon climate zones, while it could represent vegetation composition for entirely different seasons in low-latitude or polar regions (Zamanian et al., 2016; Kelson et al., 2020).

Supplementary Material. The supplementary material for this article can be found at https://doi.org/10.1017/qua.2023.66

REFERENCES

Agrawal, S., Sanyal, P., Sarkar, A., Jaiswal, M.K., Dutta, K., 2012. Variability of Indian monsoonal rainfall over the past 100 ka and its implication for C$_3$–C$_4$ vegetational change. *Quaternary Research* 77, 159–170.

Amundson, R., Stern, L., Baisden, T., Wang, Y., 1998. The isotopic composition of soil and soil-respired CO$_2$. *Geoderma* 82, 83–114.

An, Z., Kutzbach, J.E., Prell, W.L., Porter, S.C., 2001. Evolution of Asian monsoons and phased uplift of the Himalaya–Tibetan plateau since Late Miocene times. *Nature* 411, 62–66.

An, Z.S., Huang, Y.S., Liu, W.G., Guo, Z.T., Clemens, S., Li, L., *et al.*, 2005. Multiple expansions of C$_4$ plant biomass in East Asia since 7 Ma coupled with strengthened monsoon circulation. *Geology* 33, 705–708.

Barta, G., 2011. Secondary carbonates in loess-paleosoil sequences: a general review. *Central European Journal of Geosciences* 3, 129–146.

Bayat, O., Karimzadeh, H., Eghbal, M.K., Karimi, A., Amundson, R., 2018. Calcic soils as indicators of profound Quaternary climate change in eastern Isfahan, Iran. *Geoderma* 315, 220–230.

Bereiter, B., Eggleston, S., Schmitt, J., Nehrbass-Ahles, C., Stocker, T.F., Fischer, H., Kipfstuhl, S., Chappellaz, J., 2015. Revision of the EPICA Dome C CO$_2$ record from 800 to 600 kyr before present. *Geophysical Research Letters* 42, 542–549.

Bond-Lamberty, B., Thomson, A., 2010. A global database of soil respiration data. *Biogeosciences* 7, 1915–1926.

Breecker, D.O., McFadden, L.D., Sharp, Z.D., Martinez, M., Litvak, M.E., 2012. Deep autotrophic soil respiration in shrubland and woodland ecosystems in central New Mexico. *Ecosystems* 15, 83–96.

Breecker, D.O., Sharp, Z.D., McFadden, L.D., 2009. Seasonal bias in the formation and stable isotopic composition of pedogenic carbonate in modern soils from central New Mexico, USA. *GSA Bulletin* 121, 630–640.

Cao, J.J., Zhu, C.S., Chow, J.C., Liu, W.G., Han, Y.M., Watson, J.G., 2008. Stable carbon and oxygen isotopic composition of carbonate in fugitive dust in the Chinese Loess Plateau. *Atmospheric Environment* 42, 9118–9122.

Carrapa, B., Clementz, M., Feng, R., 2019. Ecological and hydroclimate responses to strengthening of the Hadley circulation in South America during the Late Miocene cooling. *Proceedings of the National Academy of Sciences USA* 116, 9747–9752.

Cerling, T.E., 1984. The stable isotopic composition of modern soil carbonate and its relationship to climate. *Earth and Planetary Science Letters* 71, 229–240.

Cerling, T.E., Harris, J.M., MacFadden, B.J., Leakey, M.G., Quade, J., Eisenmann, V., Ehleringer, J.R., 1997. Global vegetation change through the Miocene/Pliocene boundary. *Nature* 389, 153.

Cerling, T.E., Quade, J., 1993. Stable carbon and oxygen isotopes in soil carbonates. In: Swart, P.K., Lohmann, K.C., Mckenzie, J., Savin S. (Eds,), *Climate Change in Continental Isotopic Records*. Geophysical Monograph Series 78. American Geophysical Union, Washington, DC, pp. 217–231.

Cerling, T.E., Quade, J., Wang, Y., Bowman, J.R., 1989. Carbon isotopes in soils and palaeosols as ecology and palaeoecology indicators. *Nature* 341, 138–139.

Chen, J., Li, G.J., 2011. Geochemical studies on the source region of Asian dust. *Science China Earth Sciences* 54, 1279.

Cheng, Y., Qiao, Y., Liu, Z., Li, J., Peng, S., Li, C., Qi, L., Wang, Y., 2014. Magnetostratigraphy and chorma records of a red clay formation near Lingtai County of Gansu Province. *Quaternary Sciences* 34, 391–398.

Da, J., Zhang, Y.G., Li, G., Ji, J., 2020. Aridity-driven decoupling of δ^{13}C between pedogenic carbonate and soil organic matter. *Geology* 48, 981–985.

Da, J., Zhang, Y.G., Wang, H., Balsam, W., Ji, J., 2015. An Early Pleistocene atmospheric CO$_2$ record based on pedogenic carbonate from the Chinese loess deposits. *Earth and Planetary Science Letters* 426, 69–75.

Davidson, G.R., 1995. The stable isotopic composition and measurement of carbon in soil CO$_2$. *Geochimica et Cosmochimica Acta* 59, 2485–2489.

Ding, Z.L., Yang, S.L., 2000. C$_3$/C$_4$ vegetation evolution over the last 7.0 Myr in the Chinese Loess Plateau: evidence from pedogenic carbonate δ^{13}C. *Palaeogeography, Palaeoclimatology, Palaeoecology* 160, 291–299.

Edwards, E.J., Osborne, C.P., Strömberg, C.A.E., Smith, S.A., 2010. The origins of C$_4$ grasslands: integrating evolutionary and ecosystem. *Science* 328, 587.

Ehleringer, J.R., Monson, R.K., 1993. Evolutionary and ecological aspects of photosynthetic pathway variation. *Annual Review of Ecology and Systematics* 24, 411–439.

Ehleringer, J.R., Sage, R.F., Flanagan, L.B., Pearcy, R.W., 1991. Climate change and the evolution of C$_4$ photosynthesis. *Trends in Ecology & Evolution* 6, 95–99.

Farquhar, G., O'Leary, M., Berry, J., 1982. On the relationship between carbon isotope discrimination and the intercellular carbon dioxide concentration in leaves. *Journal of Functional Plant Biology* 9, 121–137.

Farquhar, G.D., Ehleringer, J.R., Hubick, K.T., 1989. Carbon isotope discrimination and photosynthesis. *Annual Review of Plant Physiology and Plant Molecular Biology* 40, 503–537.

Feng, Z.D., Wang, H.B., 2005. Pedostratigraphy and carbonate accumulation in the last interglacial pedocomplex of the Chinese Loess Plateau. *Soil Science Society of America Journal* 69, 1094–1101.

Fischer-Femal, B.J., Bowen, G.J., 2021. Coupled carbon and oxygen isotope model for pedogenic carbonates. *Geochimica et Cosmochimica Acta* 294, 126–144.

Ghosh, S., Sanyal, P., Sangode, S.J., Nanda, A.C., 2018. Substrate control of C$_4$ plant abundance in the Himalayan foreland: a study based on inter-basinal records from Plio-Pleistocene Siwalik Group sediments. *Palaeogeography, Palaeoclimatology, Palaeoecology* 511, 341–351.

Guo, Z., Peng, S., Hao, Q., Biscaye, P.E., An, Z., Liu, T., 2004. Late Miocene–Pliocene development of Asian aridification as recorded in the Red-Earth Formation in northern China. *Global and Planetary Change* 41, 135–145.

Hanson, P.J., Edwards, N.T., Garten, C.T., Andrews, J.A., 2000. Separating root and soil microbial contributions to soil respiration: a review of methods and observations. *Biogeochemistry* 48, 115–146.

Hao, Q., Oldfield, F., Bloemendal, J., Guo, Z., 2008. The magnetic properties of loess and paleosol samples from the Chinese Loess Plateau spanning the

last 22 million years. *Palaeogeography, Palaeoclimatology, Palaeoecology* **260**, 389–404.

Hao, Q., Oldfield, F., Bloemendal, J., Torrent, J., Guo, Z., 2009. The record of changing hematite and goethite accumulation over the past 22 Myr on the Chinese Loess Plateau from magnetic measurements and diffuse reflectance spectroscopy. *Journal of Geophysical Research: Solid Earth* **114**. https://doi.org/10.1029/2009JB006604.

Hatch, M.D., Slack, CR., 1970. Photosynthetic CO_2-fixation pathways. *Annual Review of Plant Physiology* **21**, 141–162.

Horton, T.W., Defliese, W.F., Tripati, A.K., Oze, C., 2016. Evaporation induced ¹⁸O and ¹³C enrichment in lake systems: a global perspective on hydrologic balance effects. *Quaternary Science Reviews* **131**, 365–379.

Huth, T.E., Cerling, T.E., Marchetti, D.W., Bowling, D.R., Ellwein, A.L., Passey, B.H., 2019. Seasonal bias in soil carbonate formation and its implications for interpreting high-resolution paleoarchives: evidence from southern Utah. *Journal of Geophysical Research: Biogeosciences* **124**, 616–632.

[IAEA/WMO] International Atomic Energy Agency/World Meteorological Organization, 2006. Global Network of Isotopes in Precipitation. GNIP Database. https://nucleus.iaea.org/wiser.

Jiang, H., Ding, Z., 2005. Temporal and spatial changes of vegetation cover on the Chinese Loess Plateau through the last glacial cycle: evidence from spore-pollen records. *Review of Palaeobotany and Palynology* **133**, 23–37.

Jiang, W., Cheng, Y., Yang, X., Yang, S., 2013. Chinese Loess Plateau vegetation since the Last Glacial Maximum and its implications for vegetation restoration. *Journal of Applied Ecology* **50**, 440–448.

Jiang, W., Han, J., Liu, T.S., 2001. Aridification and its influence on carbon isotope composition of pedogenic carbonate. *Quaternary Sciences* **21**, 427–435.

Jiang, W., Wu, H., Li, Q., Lin, Y., Yu, Y., 2019. Spatiotemporal changes in C_4 plant abundance in China since the Last Glacial Maximum and their driving factors. *Palaeogeography, Palaeoclimatology, Palaeoecology* **518**, 10–21.

Kelson, J.R., Huntington, K.W., Breecker, D.O., Burgener, L.K., Gallagher, T.M., Hoke, G.D., Petersen, S.V., 2020. A proxy for all seasons? A synthesis of clumped isotope data from Holocene soil carbonates. *Quaternary Science Reviews* **234**, 106259.

Kovda, I., Morgun, E., Gongalsky, K., 2014. Stable isotopic composition of carbonate pedofeatures in soils along a transect in the southern part of European Russia. *Catena* **112**, 56–64.

Kukla, G., Heller, F., Liu, X.M., Tong, S.C., Liu, T.S., S., A.Z., 1988. Pleistocene climates in China dated by magnetic susceptibility. *Geology* **16**, 811–814.

Lai, C.-T., Riley, W., Owensby, C., Ham, J., Schauer, A., Ehleringer, J.R., 2006. Seasonal and interannual variations of carbon and oxygen isotopes of respired CO_2 in a tallgrass prairie: measurements and modeling results from 3 years with contrasting water availability. *Journal of Geophysical Research: Atmospheres* **111**. https://doi.org/10.1029/2005JD006436.

Li, G., Chen, J., Chen, Y., 2013. Primary and secondary carbonate in Chinese loess discriminated by trace element composition. *Geochimica et Cosmochimica Acta* **103**, 26–35.

Li, G., Sheng, X., Chen, J., Yang, J., Chen, Y., 2007. Oxygen-isotope record of paleorainwater in authigenic carbonates of Chinese loess-paleosol sequences and its paleoclimatic significance. *Palaeogeography, Palaeoclimatology, Palaeoecology* **245**, 551–559.

Li, T., Li, G., 2014. Incorporation of trace metals into microcodium as novel proxies for paleo-precipitation. *Earth and Planetary Science Letters* **386**, 34–40.

Li, X., Fang, X., Wu, F., Miao, Y., 2011. Pollen evidence from Baode of the northern Loess Plateau of China and strong East Asian summer monsoons during the Early Pliocene. *Chinese Science Bulletin* **56**, 64–69.

Liu, W.G., Huang, Y.S., An, Z.S., Clemens, S.C., Li, L., Prell, W.L., Ning, Y.F., 2005. Summer monsoon intensity controls C_4/C_3 plant abundance during the last 35 ka in the Chinese Loess Plateau: carbon isotope evidence from bulk organic matter and individual leaf waxes. *Palaeogeography, Palaeoclimatology, Palaeoecology* **220**, 243–254.

Liu, W.G., Yang, H., Sun, Y.B., Wang, X.L., 2011. δ¹³C Values of loess total carbonate: a sensitive proxy for Asian summer monsoon in arid northwestern margin of the Chinese loess plateau. *Chemical Geology* **284**, 317–322.

Luo, X., Wang, H., An, Z., Zhang, Z., Liu, W., 2020. Carbon and oxygen isotopes of calcified root cells, carbonate nodules and total inorganic carbon in

the Chinese loess–paleosol sequence: the application of paleoenvironmental studies. *Journal of Asian Earth Sciences* **201**, 104515.

Lv, Y., Chunxia, Z., Fu, Y., Wu, H., Hao, Q., Qiao, Y., Guo, Z., 2022. Clay mineralogical and geochemical record from a loess-paleosol sequence in Chinese Loess Plateau during the past 880 ka and the implication on the East Asian Summer Monsoon. *Quaternary Sciences* **42**, 921–938.

Ma, Y., Wu, F., Fang, X., Li, J., An, Z., Wang, W., 2005. Pollen record from red clay sequence in the central Loess Plateau between 8.10 and 2.60 Ma. *Chinese Science Bulletin* **50**, 2234–2243.

Maeda, H.A., Fernie, A.R., 2021. Evolutionary History of Plant Metabolism. *Annual Review of Plant Biology* **72**, 185–216.

Meng, X., Liu, L., Balsam, W., Li, S., He, T., Chen, J., Ji, J., 2015. Dolomite abundance in Chinese loess deposits: a new proxy of monsoon precipitation intensity. *Geophysical Research Letters* **42**, 10391–310398.

Meng, X., Liu, L., Zhao, W., He, T., Chen, J., Ji, J., 2019. Distant Taklimakan Desert as an important source of aeolian deposits on the Chinese Loess Plateau as evidenced by carbonate minerals. *Geophysical Research Letters* **46**, 4854–4862.

Monger, H.C., Cole, D.R., Buck, B.J., Gallegos, R.A., 2009. Scale and the isotopic record of C_4 plants in pedogenic carbonate: from the biome to the rhizosphere. *Ecology* **90**, 1498–1511.

Montañez, I.P., 2013. Modern soil system constraints on reconstructing deep-time atmospheric CO_2. *Geochimica et Cosmochimica Acta* **101**, 57–75.

Munroe, S.E.M., McInerney, F.A., Guerin, G.R., Andrae, J.W., Welti, N., Caddy-Retalic, S., Atkins, R., Sparrow, B., 2022. Plant families exhibit unique geographic trends in C_4 richness and cover in Australia. *PLoS ONE* **17**, e0271603.

Myers, T.S., Tabor, N.J., Jacobs, L.L., Bussert, R.J.J.o.S.R., 2016. Effects of different organic-matter sources on estimates of atmospheric and soil pCO2 using pedogenic carbonate. *Journal of Sedimentary Research* **86**, 800–812.

Nie, J., King, J.W., Fang, X., 2007. Enhancement mechanisms of magnetic susceptibility in the Chinese red-clay sequence. *Geophysical Research Letters* **34**. https://doi.org/10.1029/2007GL031430.

O'Leary, M.H., 1981. Carbon isotope fractionation in plants. *Phytochemistry* **20**, 553–567.

Pearcy, R.W., Ehleringer, J., 1984. Comparative ecophysiology of C_3 and C_4 plants. *Plant, Cell & Environment* **7**, 1–13.

Peters, N.A., Huntington, K.W., Hoke, G.D., 2013. Hot or not? Impact of seasonally variable soil carbonate formation on paleotemperature and O-isotope records from clumped isotope thermometry. *Earth and Planetary Science Letters* **361**, 208–218.

Qi, L., Qiao, Y., Liu, Z., Wang, Y., Peng, S., 2021. Geochemical characteristics of the Tertiary and Quaternary eolian deposits in eastern Gansu Province: implications for provenance and weathering intensity. *Journal of Geomechanics* **27**, 475.

Quade, J., Rech, J.A., Latorre, C., Betancourt, J.L., Gleeson, E., Kalin, M.T.K., 2007. Soils at the hyperarid margin: the isotopic composition of soil carbonate from the Atacama Desert, northern Chile. *Geochimica et Cosmochimica Acta* **71**, 3772–3795.

Rae, J.W.B., Zhang, Y.G., Liu, X., Foster, G.L., Stoll, H.M., Whiteford, R.D.M., 2021. Atmospheric CO_2 over the past 66 million years from marine archives. *Annual Review of Earth and Planetary Sciences* **49**, 609–641.

Rao, Z., Chen, F., Zhang, X., Xu, Y., Xue, Q., Zhang, P., 2012b. Spatial and temporal variations of C_3/C_4 relative abundance in global terrestrial ecosystem since the Last Glacial and its possible driving mechanisms. *Chinese Science Bulletin* **57**, 4024–4035.

Rao, Z., Zhu, Z., Chen, F., Zhang, J., 2006. Does δ¹³C_Carb of the Chinese loess indicate past C_3/C_4 abundance? A review of research on stable carbon isotopes of the Chinese loess. *Quaternary Science Reviews* **25**, 2251–2257.

Rao, Z.G., Guo, W.K., Cao, J.T., Shi, F.X., Jiang, H., Li, CZ, 2017. Relationship between the stable carbon isotopic composition of modern plants and surface soils and climate: a global review. *Earth-Science Reviews* **165**, 110–119.

Rao, Z.G., Zhang, X., Xue, Q., Xu, Y., Liu, X., 2012a. Primary organic carbon isotopic study result of Xifeng loess/red clay profile. *Quaternary Sciences* **32**, 825–827.

Retallack, G.J., 2005. Pedogenic carbonate proxies for amount and seasonality of precipitation in paleosols. *Geology* 33, 333–336.

Retallack, G.J., 2009. Refining a pedogenic-carbonate CO_2 paleobarometer to quantify a middle Miocene greenhouse spike. *Palaeogeography, Palaeoclimatology, Palaeoecology* 281, 57–65.

Romanek, C.S., Grossman, E.L., Morse, J.W., 1992. Carbon isotopic fractionation in synthetic aragonite and calcite: effects of temperature and precipitation rate. *Geochimica et Cosmochimica Acta* 56, 419–430.

Sage, R.F., Sage, T.L., Kocacinar, F., 2012. Photorespiration and the evolution of C_4 photosynthesis. *Annual Review of Plant Biology* 63, 19–47.

Sanyal, P., Sarkar, A., Bhattacharya, S.K., Kumar, R., Ghosh, S.K., Agrawal, S., 2010. Intensification of monsoon, microclimate and asynchronous C_4 appearance: isotopic evidence from the Indian Siwalik sediments. *Palaeogeography, Palaeoclimatology, Palaeoecology* 296, 165–173.

Sarangi, V., Agrawal, S., Sanyal, P., 2021. The disparity in the abundance of C_4 plants estimated using the carbon isotopic composition of paleosol components. *Palaeogeography, Palaeoclimatology, Palaeoecology* 561, 110068.

Schmitt, J., Schneider, R., Elsig, J., Leuenberger, D., Lourantou, A., Chappellaz, J., Köhler, P., et al., 2012. Carbon isotope constraints on the deglacial CO_2 rise from ice cores. *Science* 336, 711–714.

Sheldon, N.D., Tabor, N.J., 2009. Quantitative paleoenvironmental and paleoclimatic reconstruction using paleosols. *Earth-Science Reviews* 95, 1–52.

Sheng, X.F., Chen, J., Ji, J.F., Chen, T.H., Li, G.J., Teng, H.H., 2008. Morphological characters and multi-element isotopic signatures of carbonates from Chinese loess–paleosol sequences. *Geochimica et Cosmochimica Acta* 72, 4323–4337.

Shimoda, S., Murayama, S., Mo, W., Oikawa, T., 2009. Seasonal contribution of C_3 and C_4 species to ecosystem respiration and photosynthesis estimated from isotopic measurements of atmospheric CO_2 at a grassland in Japan. *Agricultural and Forest Meteorology* 149, 603–613.

Shu, P., Wang, H., Zhou, W., Ao, D., Niu, D., Wen, X., Li, B., 2021. Seasonal rainfall patterns in stable carbon isotopes in the Mu Us Desert, northern China during the early and middle Holocene. *Climate Dynamics* 56, 799–812.

Sinha, R., Tandon, S.K., Sanyal, P., Gibling, M.R., Stuben, D., Berner, Z., Ghazanfari, P., 2006. Calcretes from a Late Quaternary interfluve in the Ganga Plains, India: carbonate types and isotopic systems in a monsoonal setting. *Palaeogeography, Palaeoclimatology, Palaeoecology* 242, 214–239.

Stevenson, B.A., Kelly, E.F., McDonald, E.V., Busacca, A.J., 2005. The stable carbon isotope composition of soil organic carbon and pedogenic carbonates along a bioclimatic gradient in the Palouse region, Washington State, USA. *Geoderma* 124, 37–47.

Suarez, M.B., Passey, B.H., Kaakinen, A., 2011. Paleosol carbonate multiple isotopologue signature of active East Asian summer monsoons during the late Miocene and Pliocene. *Geology* 39, 1151–1154.

Sun, J.M., Lü, T.Y., Zhang, Z.Q., Wang, X., Liu, W.G., 2012. Stepwise expansions of C_4 biomass and enhanced seasonal precipitation and regional aridity during the Quaternary on the southern Chinese Loess Plateau. *Quaternary Science Reviews* 34, 57–65.

Sun, Y., An, Z., Clemens, S.C., Bloemendal, J., Vandenberghe, J., 2010. Seven million years of wind and precipitation variability on the Chinese Loess Plateau. *Earth and Planetary Science Letters* 297, 525–535.

Sun, Y., Kutzbach, J., An, Z., Clemens, S., Liu, Z., Liu, W., Liu, X., et al., 2015. Astronomical and glacial forcing of East Asian summer monsoon variability. *Quaternary Science Reviews* 115, 132–142.

Sun, Y., Yin, Q., Crucifix, M., Clemens, S.C., Araya-Melo, P., Liu, W., Qiang, X., et al., 2019. Diverse manifestations of the mid-Pleistocene climate transition. *Nature Communications* 10, 352.

Thomas, B., 1991. Stable carbon isotope ratios of natural materials: I. Sample preparation and mass spectrometric analysis. In: Paul, E., Melillo, J. (Eds.), *Carbon Isotope Techniques*. Elsevier, Amsterdam, pp. 155–172.

Tipple, B.J., Meyers, S.R., Pagani, M., 2010. Carbon isotope ratio of Cenozoic CO_2: a comparative evaluation of available geochemical proxies. *Paleoceanography* 25. https://doi.org/10.1029/2009PA001851.

Tipple, B.J., Pagani, M., 2007. The early origins of terrestrial C_4 photosynthesis. *Annual Review of Earth and Planetary Sciences* 35, 435–461.

Tribble, J.S., Arvidson, R.S., Lane, M., Mackenzie, F.T., 1995. Crystal chemistry, and thermodynamic and kinetic properties of calcite, dolomite, apatite, and biogenic silica: applications to petrologic problems. *Sedimentary Geology* 95, 11–37.

Vögeli, N., Najman, Y., van der Beek, P., Huyghe, P., Wynn, P.M., Govin, G., van der Veen, I., Sachse, D., 2017. Lateral variations in vegetation in the Himalaya since the Miocene and implications for climate evolution. *Earth and Planetary Science Letters* 471, 1–9.

Von Fischer, J.C., Tieszen, L.L., Schimel, D.S., 2008. Climate controls on C_3 vs. C_4 productivity in North American grasslands from carbon isotope composition of soil organic matter. *Global Change Biology* 14, 1141–1155.

Vuille, M., Werner, M., Bradley, R.S., Keimig, F., 2005. Stable isotopes in precipitation in the Asian monsoon region. *Journal of Geophysical Research: Atmospheres* 110. https://doi.org/10.1029/2005JD006022.

Wang, G., Feng, X., Han, J., Zhou, L., Tan, W., Su, F., 2008. Paleovegetation reconstruction using $\delta^{13}C$ of soil organic matter. *Biogeosciences* 5, 1325–1337.

Wang, H., Ambrose, S.H., Fouke, B.W., 2004. Evidence of long-term seasonal climate forcing in rhizolith isotopes during the last glaciation. *Geophysical Research Letters* 31. https://doi.org/10.1029/2004GL020207.

Wang, H., Follmer, L.R., 1998. Proxy of monsoon seasonality in carbon isotopes from paleosols of the southern Chinese Loess Plateau. *Geology* 26, 987–990.

Wang, R., Ma, L., 2016. Climate-driven C_4 plant distributions in China: divergence in C_4 taxa. *Scientific Reports* 6, 27977.

Wang, Y.Q., Zhang, X.Y., Arimoto, R., Cao, J.J., Shen, Z.X., 2005. Characteristics of carbonate content and carbon and oxygen isotopic composition of northern China soil and dust aerosol and its application to tracing dust sources. *Atmospheric Environment* 39, 2631–2642.

Yang, S.L., Ding, Z.L., 2008. Advance–retreat history of the East-Asian summer monsoon rainfall belt over northern China during the last two glacial–interglacial cycles. *Earth and Planetary Science Letters* 274, 499–510.

Yang, S.L., Ding, Z.L., Li, Y.Y., Wang, X., Jiang, W.Y., Huang, X.F., 2015. Warming-induced northwestward migration of the East Asian monsoon rain belt from the Last Glacial Maximum to the mid-Holocene. *Proceedings of the National Academy of Sciences USA* 112, 13178–13183.

Yang, S.L., Ding, Z.L., Wang, X., Tang, Z.H., Gu, Z.Y., 2012. Negative $\delta^{18}O$–$\delta^{13}C$ relationship of pedogenic carbonate from northern China indicates a strong response of C_3/C_4 biomass to the seasonality of Asian monsoon precipitation. *Palaeogeography, Palaeoclimatology, Palaeoecology* 317–318, 32–40.

Zamanian, K., Pustovoytov, K., Kuzyakov, Y., 2016. Pedogenic carbonates: forms and formation processes. *Earth-Science Reviews* 157, 1–17.

Zhang, H., Lu, H., He, J., Xie, W., Wang, H., Zhang, H., Breecker, D., et al., 2022. Large-number detrital zircon U-Pb ages reveal global cooling caused the formation of the Chinese Loess Plateau during Late Miocene. *Science Advances* 8, eabq2007.

Zhang, P., Liu, W., 2013. Carbon isotope composition and paleoenvironment information of rhizolith in Xifeng and Luochuan loess. *Quaternary Sciences* 33, 179–186.

Zhang, P., Liu, W.G., Qiang, X.K., 2013a. Vegetation coverage and monsoon variation recorded by stable carbon isotope of loes since 2.5Ma. *Marine Geology & Quaternary Geology* 33, 137–143.

Zhang, Z., Li, G., Yan, H., An, Z., 2018. Microcodium in Chinese loess as a recorder for the oxygen isotopic composition of monsoonal rainwater. *Quaternary International* 464, 364–369.

Zhou, B., Shen, C.D., Sun, W.D., Bird, M., Ma, W.T., Taylor, D., Liu, W.G., Peterse, F., Yi, W.X., Zheng, H.B., 2014. Late Pliocene–Pleistocene expansion of C_4 vegetation in semi-arid East Asia linked to increased burning. *Geology* 42, 1067–1070.

Zhou, L.P., Oldfield, F., Wintle, A.G., Robinson, S.G., Wang, J.T., 1990. Partly pedogenic origin of magnetic variations in Chinese loess. *Nature* 346, 737–739.